Numerical and experimental investigation of FBG strain response at cryogenic temperatures

V. N. Venkatesan, R. Ramalingam

Institute of Technical Physics (ITEP), Karlsruhe Institute of Technology (KIT), Germany

rajini-kumar.ramalingam@kit.edu

Abstract. Strain response of FBG sensors are investigated at various temperatures from 298 K to 4.2 K. Numerical modelling is carried out for acrylate coated, substrate-free fiber Bragg grating (FBG) sensors at room temperature of 298 K and cryogenic temperatures of 77 K, 10 K and 4.2 K. A 1550 nm Bragg wavelength (λ_B) FBG sensor is modelled and simulated for applied strain (ε) ranging from 0 to 800 µm/m. The Bragg wavelength shifts ($\Delta\lambda_B$) thus obtained are compared with the experimentally investigated values obtained by subjecting the FBG sensor to axial strain, with its sensing part not being bonded to any surface. The MTS25 tensile machine with a cryostat under vacuum conditions (10^{-4} mbar pressure) is used for the experiments and the required temperatures are maintained using liquid Nitrogen (LN_2) and compressed Helium gas (He). The Bragg wavelength shift ($\Delta\lambda_B$) versus induced strain (ε) is regressed with a linear polynomial function and the strain sensitivity obtained in both the cases are discussed.

1. Introduction

Fiber Bragg gratings (FBG) are considered one of the most reliable sensors to monitor crucial process parameters like pressure, temperature, flowrate, concentration, etc [1-4], thanks to their miniature size, high sensitivity, electrical and magnetic immunity, and multiplexing capabilities. FBG sensors prove to be a good replacement for the conventional sensors, especially for measurements at cryogenic temperatures [5-8]. As well documented in literature [9-11], FBG is a short segment in the core of an optical fiber which has a periodic variation of refractive index. The gratings are inscribed into the optical fiber using UV interferometer [12]. Due to the varying refractive index of the FBG, one particular wavelength of the incident light is reflected and the others are transmitted, as depicted in Figure 1. This reflected wavelength (central wavelength of the reflected band) is called the Bragg wavelength (λ_B) and it satisfies the following condition [13]:

$$\lambda_B = 2\Lambda n_{eff} \tag{1}$$

where Λ and n_{eff} are the grating period and effective refractive index of the FBG, respectively.

Any thermal or mechanical strain caused on the FBG will alter its Bragg wavelength due to photo-elastic and thermo-optic effects, thus enabling its application in measurement technology. The change in wavelength is called the Bragg wavelength shift ($\Delta\lambda_B$) and is expressed as [13]:

$$\frac{\Delta\lambda_B}{\lambda_B} = (\alpha_s + \alpha_e)\Delta T + (1 - p_e)\varepsilon \tag{2}$$

Content from this work may be used under the terms of the Creative Commons Attribution 3.0 licence. Any further distribution of this work must maintain attribution to the author(s) and the title of the work, journal citation and DOI.
Published under licence by IOP Publishing Ltd

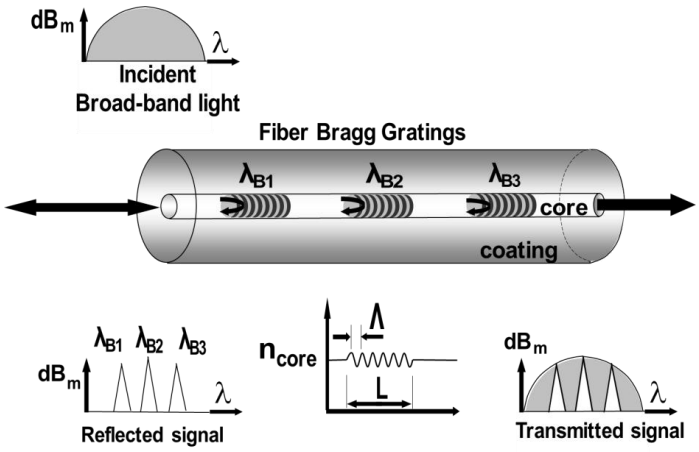

Figure 1. Principle of Fiber Bragg Gratings.

where ΔT is the temperature difference, ε the strain, α_s the thermal expansion coefficient (0.55×10^{-6} for silica), α_e the thermo-optic coefficient (8.6×10^{-6} for silica), and p_e the effective strain-optic coefficient of the fiber which can be calculated using [13]:

$$p_e = \frac{n^2}{2}\left[p_{12} - \nu\left(p_{11} + p_{12}\right)\right] \tag{3}$$

where p_{11} and p_{12} are the components of strain-optic tensor, n the fiber core refractive index, and ν the Poisson's ratio. For a typical FBG sensor ($p_{11} = 0.113$, $p_{12} = 0.252$, $\nu = 0.16$ and $n = 1.482$), p_e is 0.22. For a Bragg wavelength ~1550 nm, the expected strain sensitivity is 1.2 pm/με, i.e., for an applied strain of 1 με, the change in Bragg wavelength will be 1.2 pm. The expected temperature sensitivity is 13.7 pm/K. The strain and temperature sensitivities of the FBG, however, vary from sensor to sensor, thus requiring a calibration before any measurement.

Strain and temperature response of FBG sensors are investigated and reported regularly [14-16]. The reported strain sensitivities, however, vary depending on many factors like the type of FBG sensor, strain transfer efficiency, gluing techniques used, etc., making it difficult to draw conclusions on the actual sensor response. This leads to the importance of studying the strain response without attaching the FBG sensing part to any surface. To the best of our knowledge, investigations of un-bonded or substrate-free FBG sensors at cryogenic temperatures have not been reported so far. This paper discusses the numerical and experimental investigation of a substrate-free FBG sensor at various temperatures whose sensing part is not attached to any surface.

2. Numerical Investigation

Numerical simulation is performed to study the strain response of an acrylate coated single mode FBG sensor using COMSOL 4.4, a commercial finite element analysis software. A 3D linear elastic solid mechanics model of the FBG sensor is assumed as the strain range to be studied (0 to 800 μm/m) is well within its elastic limit. The purpose is to obtain the Bragg wavelength shift ($\Delta\lambda_B$) for the given strain (ε) and it is done based on Equation 2 and 3, which are fed to the solver. The values of α_s, α_e, p_{11} and p_{12} are obtained from the solver's database based on the material properties of the optical fiber.

The geometry of the model considered consists of two concentric cylinders (Figure 2) which represent the core and coating of the FBG optical fiber respectively, whose specifications are given in Table 1. The physical properties tabled are at 298 K and the solver calculates for the other temperatures depending on the material. As silica is a fragile material with high Young's modulus of 7.33×10^{10}, a more elastic acrylate polymer coating with Young's modulus 2.5×10^{9} is provided around the core to provide high strength and flexibility to the FBG.

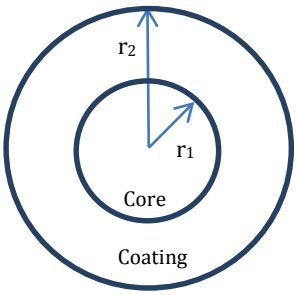

Figure 2. Optical fiber schematic.

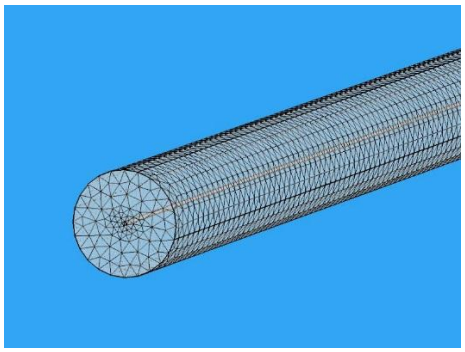

Figure 3. Tetragonal meshing drawn on the core and coating.

A tetrahedral mesh (Figure 3) with non-uniform grid spacing is generated for the geometry. At the region near the core, the grid spacing is much finer than the region away from it. This is done to ensure high accuracy as the material properties change between the core and the coating.

Table 1. FBG core and coating specifications.

Core	Material	Silica
	Shear modulus (G_1)	3.01×10^{10} Pa
	Young's modulus (E_1)	7.33×10^{10} Pa
	Thermo-optic coefficient (α_e)	8.60×10^{-6} K^{-1}
	Thermal expansion coefficient (α_s)	5.50×10^{-7} K^{-1}
	Strain-optic coefficient (P_e)	0.22
	Bragg wavelength (λ_B)	1550 nm
	Diameter (d_1)	9.00×10^{-6} m
Coating	Material	Acrylate polymer
	Shear modulus (G_2)	1.30×10^{9} Pa
	Young's modulus (E_2)	2.50×10^{9} Pa
	Diameter (d_2)	1.95×10^{-4} m

Numerical investigation is performed by prescribing a displacement to one end and assuming the other end to be stationery. The displacement values (ΔL) to be provided correspond to the user-required strain values (ε) which are calculated by:

$$\varepsilon = \frac{\Delta L}{L} \tag{4}$$

where L is the length of the sensor subjected to strain. For the given strain values ranging from 0 to 800 μm/m, steady state simulation is carried out for the temperatures of 298 K, 77 K, 10 K and 4.2 K. The Bragg wavelength shift data obtained from the numerical simulation are plotted against the corresponding strain and compared with those obtained from the experiment. The numerical simulation results are discussed along with the experimental results in the 4th section.

3. Experimental investigation

A commercial polyamide coated single mode fiber (SMF 28) consisting of two FBG sensors is used in this investigation. Each FBG has a different spatial period, thus having different Bragg wavelengths,

namely, λ_{B1} and λ_{B2}. The ends of one sensor (FBG 1) are glued firmly to two stainless steel structures, making sure that the FBG sensing part is free and does not have any contact with any surface (Figure 4). FBG 1 can sense both strain and temperature. The other sensor (FBG 2) is let to hang freely to ensure that there is no strain felt in it and is used to sense only temperature.

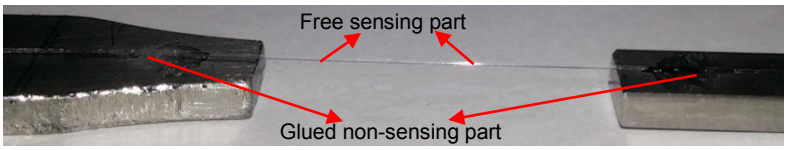

Figure 4. FBG 1 glued to metal structures with the central sensing part not touching any surface.

The ends of FBG 1 are glued to the metal structures using epoxy-phenol adhesive. This type of adhesive requires a heat treatment at about 160 ^{0}C for 2 hours. The heated sample is allowed to cool naturally till it reaches the room temperature. The spectra of FBG 1 before and after the heat treatment is plotted in Figure 5. It can be seen that the spectral pattern is almost the same and there is no significant change in the initial Bragg wavelength. Thus, the chosen heat treatment has not affected the FBG sensor properties.

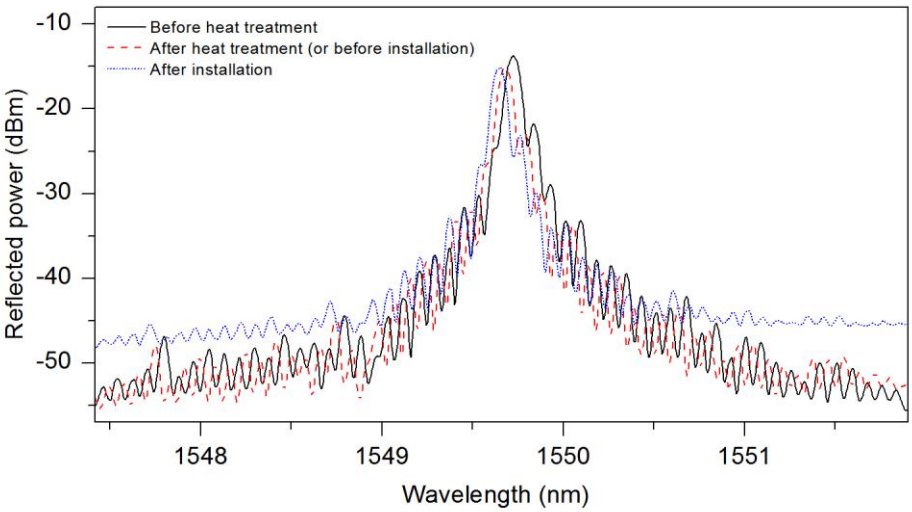

Figure 5. Spectral comparison of FBG before heat treatment, after heat treatment (same for pre-installation) and after installation.

The sample is then transferred to the MTS25 tensile machine with cryostat available at Cryogenic Material tests Karlsruhe (CryoMaK) [17], ITeP, KIT. The tensile machine consists of an extensometer (also called top load cell) and a bottom load cell. An extensometer is a device that is used to measure the distance between two distinct points on the surface of the attached specimen [18, 19]. A calibrated extensometer is used as a reference sensor for the tests. The metal structures with fiber are installed by attaching to the load cells (Figure 6) of the tensile machine, which has an accuracy of ±1 μm displacement. A pre-strain is given to the sensor to avoid errors in measurement due to bending of the sensor. To ensure that the installation has not affected the FBG properties, the spectral data before and after installation are also compared. Figure 5 shows that the Bragg wavelength of the sensor is almost equal before the installation (same as post-heat treatment) and after the installation of the sensor between the load cells.

Keeping the top load cell (extensometer) fixed, the bottom load cell is moved by the displacement bellow (works on hydraulic mechanism) under it for the given displacement values in the command. The given displacement is completely transferred to the FBG sensor, i.e., the change in length of the sensor is equal to the displacement. This induces a strain in the FBG sensor (FBG 1), which in turn causes a Bragg wavelength shift in it. Any temperature changes around it also adds to its Bragg shift ($\Delta\lambda_{B1}$). On the other hand, the Bragg wavelength shift of FBG 2 ($\Delta\lambda_{B2}$) which hangs freely in the cryostat is caused only due to the temperature changes. Hence, temperature effects on FBG 1 can be nullified using FBG 2. After each displacement command it is necessary to wait for about five minutes for the bellow to settle down to the desired displacement. The calibration tests are first performed at room temperature for both straining (downward displacement of bottom load cell) and de-straining (upward movement of bottom load cell). The experiment is performed 3 times to test the repeatability of the sensor. For calibration tests at the desired cryogenic temperature (77 K), the test chamber (cryostat) is cooled down by the attached Liquid Nitrogen (LN_2) pipe up to 100 K. The temperature inside the chamber is monitored using a Si diode (Omega Inc., CYD 208 thermometer). To further cool the cryostat down to 77 K, compressed Helium (He) flow is started inside the pipe attached to the Cu-heat exchanger in the cryostat. Once the temperature reaches 77 K, the He flow is reduced to maintain the temperature constant.

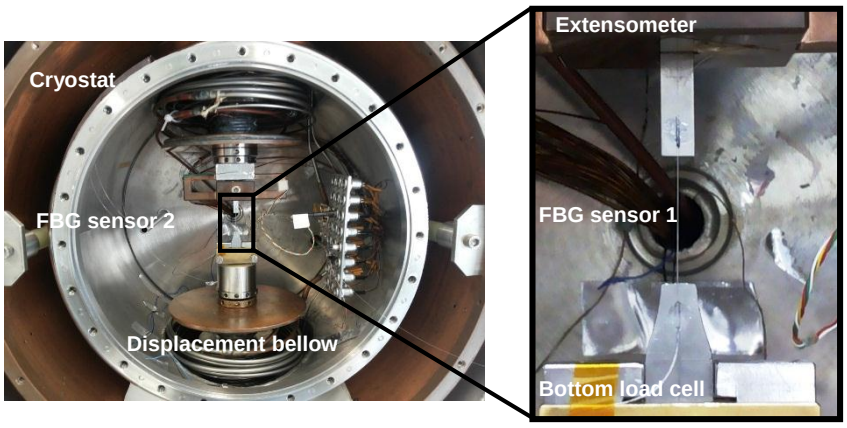

Figure 6. The sample loaded in the calibration device MTS 25 in a cryostat (left) and the FBG sensor attached to the metal structures is zoomed in for a clear view.

As there are a lot of sources of heat transfer in the cryostat, the temperature might increase if He flow is stopped. Hence, it is important to make sure He flow is continuously regulated to maintain a constant temperature of 77 K. The pressure in the cryostat is maintained at 10^{-4} mbar during the cooling down process. The investigation/calibration procedure used at 298 K is repeated for measurements at 77 K. The values of Bragg wavelength shift, displacement, extensometer voltage and temperature are recorded for each given displacement for both 298 K and 77 K. An industrial Braggmeter (FS22 Industrial BraggMETER SI) [20] is used to read the signal from FBGs. It has a very good resolution of 1.0 pm and absolute accuracy of ± 2.0 pm. In other words, temperature can be measured with an accuracy of 0.2 K and strain with 1.7 με. The Braggmeter also has good repeatability of ± 1.0 pm, showing that the error in measurement due to the measuring device is negligible.

4. Results & discussion

The respective results from the simulation and experiment are individually discussed first and then a comparison is made to describe the reliability of the FBG sensor.

For the given strain values, the Bragg wavelength shifts obtained from the simulation for temperatures of 298 K, 77 K, 10 K and 4.2 K are plotted in Figure 7. The results obtained converged with a tolerance of 10^{-3}. As it can be observed, all the values fall on a near-linear line, proving the linear dependence of Bragg shift with respect to strain. It can also be seen that the Bragg shift is almost the same for all the temperatures up to 250 µm/m strain. A negligible difference occurs for strain greater than that which could be due to small changes in the material properties at different temperatures.

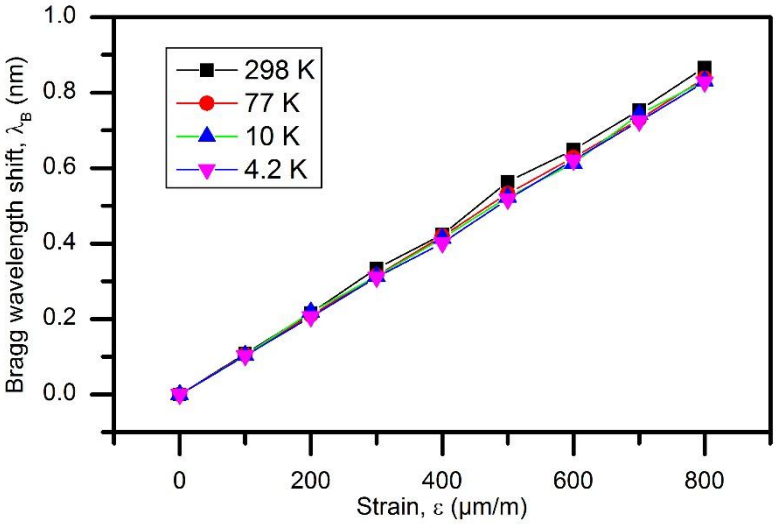

Figure 7. Numerical results of Bragg wavelength shift for corresponding induced strain values at 298 K, 77 K, 10 K and 4.2 K.

The response observed from the experiment is discussed herewith. For each given displacement, the corresponding mechanical strain is calculated based on the attached length of the fiber (L) using Equation 4. The initial length of the sensor and the corresponding initial Bragg wavelength are taken after providing the sensor with some pre-strain, to ensure that there is no error in the length due to bending of the sensor. The purely strain-dependent Bragg wavelength shift ($\Delta\lambda_B$) is given by the difference of Bragg shift of FBG 1 and FBG 2 as follows:

$$\Delta\lambda_B = \left|\Delta\lambda_{B1} - \Delta\lambda_{B2}\right| \tag{5}$$

This Bragg wavelength shift is taken on the y-axis and the induced strain is taken on the x-axis as shown Figure 8. The displacement is increased (straining) in steps of 4 µm up to 16 µm, with each step being held constant for 5 minutes. The sensor is then de-strained by decreasing the displacement in the steps of 4 µm back to 0 µm. Three runs for straining and de-straining were performed and the average is considered for the plot. It can be observed that the plot is almost linear with little hysteresis effect, i.e., for the same induced strain, the wavelength shifts during straining and de-straining phases are slightly different. The repeatability test showed that the Bragg wavelength shifts of all the three runs were in good agreement with each other. The average of straining and de-straining wavelength shifts for the corresponding strain values can be safely considered for comparison with the numerically obtained results.

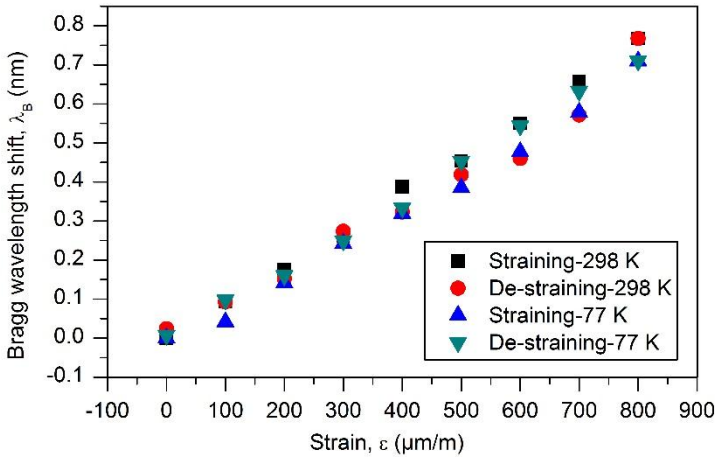

Figure 8. Bragg wavelength shift (nm) of FBG corresponding to induced strain values at 298 K and 77 K. The legends "Straining" and "De-straining" refer to the measurements performed during straining and de-straining respectively.

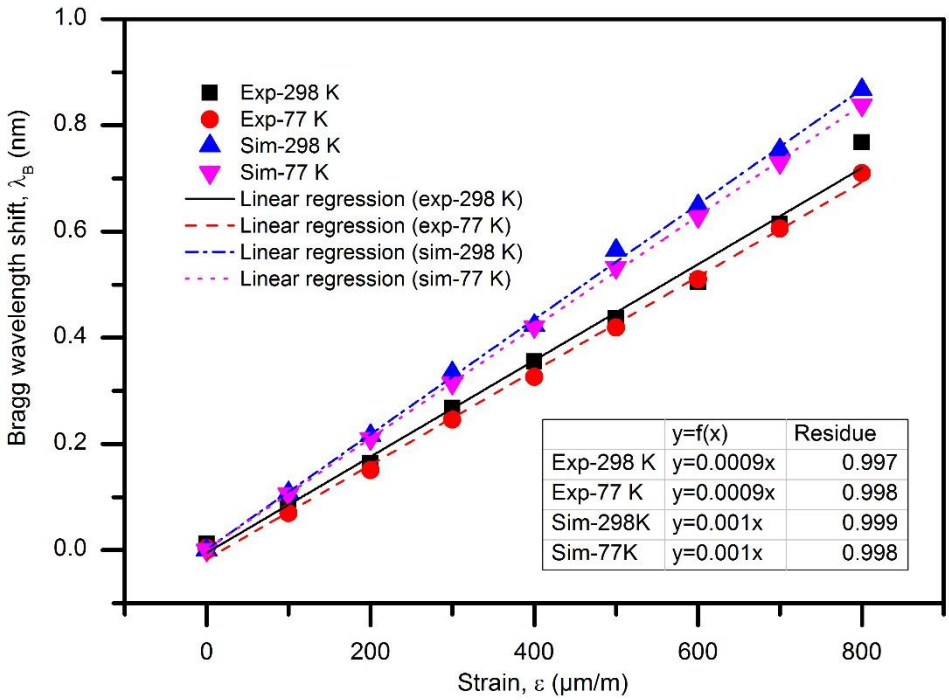

Figure 9. Experimental and simulated results of Bragg wavelength shift for corresponding induced strain values at 298 K and 77 K. Linear polynomial regression is described for all the conditions and represented by different types of line for different cases. The regression equations for Bragg wavelength shift (y in the graph) as a function of induced strain (x in the graph) are displayed.

Figure 9 gives an insight comparison of these results which has Bragg shift versus strain plots for both simulated and experimental data at 298 K and 77 K. Linear regression of all these cases are performed and it can be observed that the residual (R^2) value is very close to unity in all the cases, proving the linear dependence of Bragg shift on strain. The Bragg wavelength shift as a function of

induced strain is the same ($\Delta\lambda_B$=0.0009ε for experimental and $\Delta\lambda_B$=0.001ε for simulative) for both the cases of temperature with slightly different regression coefficients. In other words, the strain sensitivity of the FBG sensor is found to be 1 pm/με numerically, and 0.9 pm/με experimentally. This minute difference could be attributed to the strain transfer coefficient, i.e the given strain might not get completely transferred to the FBG sensor in the real case due to the presence of glue between the fiber and the metal structure.

The standard deviation between the experimentally obtained values and the regressed values is depicted in Figure 10 in the form of error bars for both the temperatures. The FBG sensor shows less error at 77 K than at 298 K. This can be attributed to the material properties of the optical fiber. It is expected to be more rigid at cryogenic temperatures, as there will be negligible vibrations in the sensor, which in turn reduces the error in measurements.

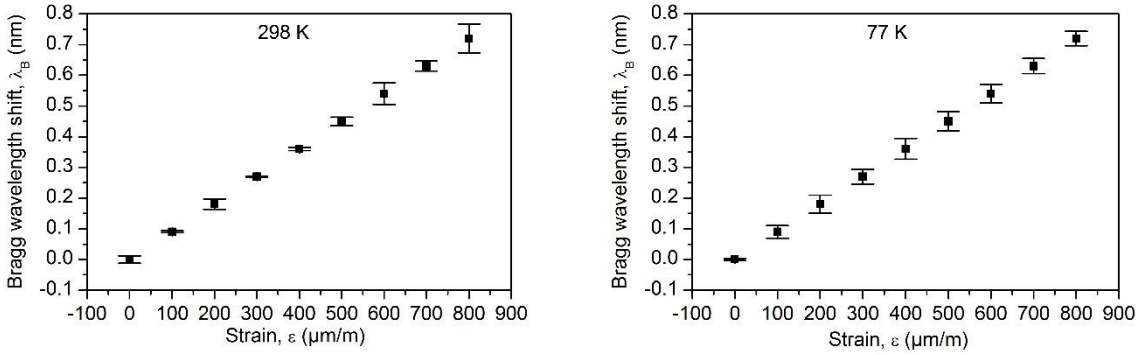

Figure 10. Error plots of FBG strain sensor between fitted and obtained values of Bragg shift at 298 K and 77 K.

As the errors obtained are negligible, the linear equation obtained by regression can be reliably used for this particular sensor. The unknown strain values can be calculated for the observed Bragg wavelength shift and thus, the strain related measurands can be estimated.

5. Conclusions

An effective numerical investigation of strain response is carried out for an FBG sensor at room temperature of 298 K and cryogenic temperatures of 77 K, 10 K and 4.2 K. Experimental test cum calibration is also done at 298 K and 77 K. This is a unique and reliable method of calibration because the sensing part of the FBG sensor is not attached to any structure or surface. The strain sensitivity of a free, acrylate coated standard FBG sensor is found to be 0.9 pm/με experimentally and 1 pm/με numerically for both the temperatures. A couple of conclusions can be drawn based on the results obtained. As reported in earlier works [14], the strain sensitivity of the FBG sensor did not depend on the temperature. The obtained results also show that the error in measurement is much less at the cryogenic temperature when compared to room temperature, thus showing that FBG sensor is highly reliable at cryogenic temperatures. This method of strain calibration of substrate-free FBG sensor has proved successful and it can be used for FBG standardization procedures.

References

[1] Rao, Y. J., "Recent progress in applications of in-fibre Bragg grating sensors," Optics and Lasers in Engineering, 31(4), 297-324 (1999).
[2] Othonos, A., Kalli, K., “Fiber Bragg Gratings – Fundamentals and application in telecommunications and sensing”, Artech House optoelectronics library (1999).
[3] Iniewski, K., "Smart sensors for industrial applications," E. d. Taylor & Francis Group, US (2013).

[4] Thekkethil, S. R., Venkatesan, V. N., Neumann, H., Ramalingam, R., "Design of cryogenic flow meter using fiber Bragg grating sensors," IEEE SENSORS 2015, 978-1-4799-8203-5 (2015).
[5] Ramalingam, R., "Fiber Bragg grating sensors for localized strain measurements at low temperature and in high magnetic field," Proc. AIP Conf., vol. 1218, no. 1, pp.1197-1204 (2010).
[6] Ramalingam, R., Neumann, H., "Fiber Bragg grating-based temperature distribution evaluation of multilayer insulations between 300 K–77 K," IEEE Sensors Journal, 11(4), 1095-1100 (2011).
[7] Ramalingam, R., Kläser, M., Schneider, T., Neumann, H., "Fiber Bragg grating sensors for strain measurement at multiple points in an NbTi superconducting sample coil," IEEE Sensors Journal, 14(3), 873-881 (2014).
[8] Bharathwaj, V., Markan, A., Atrey, M., Neumann, H., Ramalingam, R., "Fiber Bragg Gratings for distributed cryogenic temperature measurement in a tube in tube helically coiled heat exchanger," IEEE sensors 2014, Valencia, Spain, pp.1535-1538 (2014).
[9] Ramalingam, R., Nast, R., Neumann, H., "Fiber Bragg grating sensors for distributed torsional strain measurements in a (RE) BCO tape," IEEE Sensors Journal, 15(4), 2023-2030 (2015).
[10] Jicheng Li, Neumann, H., Ramalingam, R., "Design, fabrication, and testing of fiber Bragg grating sensors for cryogenic long-range displacement measurement," Cryogenics, Volume 68, June 2015, Pages 36-43, ISSN 0011-2275 (2015).
[11] Freitas, R., Araujo, F., Araujo, J., Neumann, H., Ramalingam, R., "A study on intermediate buffer layer of coated Fiber Bragg Grating cryogenic temperature sensors," IOP Conf. Series: Materials Science and Engineering, 101, 012154 (2015).
[12] Raman Kashyap "Fiber Bragg Gratings," Academic press (1999).
[13] Othonos, A., "Fiber Bragg gratings," Review of Scientific Instruments, 68, 4309-4341, (1997).
[14] Roths, J., Andrejevic, G., Kuttler, R., Süsser, M., "Calibration of Fiber Bragg cryogenic temperature sensors," 18th International Optical Fiber Sensors Conference, Optical Society of America, (2006).
[15] James, S. W., Tatam, R. P., Twin, A., Morgan, M., Noonan, P., "Strain response of fibre Bragg grating sensors at cryogenic temperatures," Measurement Science and Technology, 13, 1535-1539 (2002).
[16] Roths, J., Jülich F., "Determination of strain sensitivity of free fiber Bragg gratings," Proc. SPIE 7003, 700308, (2008).
[17] Bagrets, N., Weiss, E., Westenfelder, S., and Weiss, K-P., "Cryogenic Test Facility CryoMaK," IEEE Transactions on Applied Superconductivity, June 2012, Vol. 22, No. 3 (2012).
[18] Nyilas, A., "Strain sensing systems tailored for tensile measurement of fragile wires," Supercond. Sci. Technol. 18, S409-S415 (2005).
[19] Nyilas, A., "Transducers for sub-micron displacement measurements at cryogenic temperatures," Advances in Cryogenic Engineering: Transactions of the Cryogenic Materials Conference – ICMC, Vol. 52 (2006).
[20] FS22–Industrial BraggMETER SI, http://www.fibersensing.com/download/0b49e3852b6452701f87b4a06fa4a90d439de5b1